BMC Cardiovascular Disorders

RESEARCH

Open Access

The potential impact of exosomal miR-484 on post-myocardial infarction angiogenesis using bioinformatics and experimental verification

Dandan Wu[1,2†], Rui Yang[1†], Xu Cheng[1†], Qianqian Guo[1], Yijie Gao[1], Meng Chen[3*] and Dongmei Zhang[1*]

Abstract

Objective This study aimed to investigate the effect of miRNAs differentially expressed in serum exosomes on endothelial cells after myocardial infarction.

Design & methods Specific pathogen-free male Sprague–Dawley rats with acute myocardial infarction (AMI) were established by ligating the anterior descending branch of the left coronary artery. Hematoxylin–eosin staining was used to detect myocardial histopathological changes during model evaluation. The differentially expressed miRNAs carried by the serum exosomes were detected using the Agilent Rat miRNA Gene Chip on the Illumina platform. Gene Ontology and Kyoto Encyclopedia of Genes and Genomes pathway enrichment analyses were performed using the Database for Annotation, Visualization, and Integrated Discovery. The culture supernatant of hypoxic H9c2 cells was collected and centrifuged to obtain exosomes. The expression of miR-484 was verified using real-time fluorescence quantitative PCR (qRT–PCR). miR-484 mimics were transfected into human umbilical vein endothelial cells (HUVECs) to construct cell models of miR-484 overexpression. Cellular proliferation, scratch wound, and tube formation assays were conducted with HUVECs. A dual-luciferase reporter assay was used to validate the target gene of miR-484.

Results Serum exosomes were sequenced on an Illumina sequencing platform, and 22 differentially expressed miRNAs between the model and sham groups were detected ($P < 0.05$). Among them, miR-484 was prioritized for further evaluation, and its downregulation in MI serum exosomes was confirmed through both gene chip analysis and animal experiments. miR-484 expression increased in HUVECs after culture with exosomes from hypoxia-exposed H9c2 cells. miR-484 expression upregulation suppressed proliferation, migration, and vascular formation in HUVECs, indicating that miR-484 plays an antiangiogenic role. Bioinformatics analyses showed that rno-miR-484 and the VEGFA 3'UTR possess base binding sites. The dual-luciferase reporter assay showed that rno-miR-484 could significantly

†Dandan Wu, Rui Yang and Xu Cheng are co-authors.

*Correspondence:
Meng Chen
chinmed@yeah.net
Dongmei Zhang
chaweto@hotmail.com

Full list of author information is available at the end of the article

downregulate the expression of luciferase in r-Vegfa-3UTR-WT ($P < 0.01$). VEGFA expression was downregulated after miR-484 mimic transfection in HUVECs.

Conclusions Our study revealed that miR-484 may inhibit angiogenesis after myocardial infarction by targeting VEGFA, providing a novel focal point for the diagnosis and treatment of this disease.

Keywords Myocardial Infarction, Angiogenesis, Exosomes, miR-484, VEGF

Introduction

Myocardial infarction (MI) is an event of heart attack that occurs due to the formation of plaques in the interior walls of the arteries, resulting in myocardial damage due to hypoxia and ischemia [1]. The aggravation of myocardial injury frequently leads to heart failure and sudden death [2], making MI the main cause of morbidity and mortality worldwide. Angiogenesis is an integral and indispensable aspect of the myocardial healing process following ischemic events [3, 4], and inhibiting angiogenesis accelerates contractile dysfunction and heart failure. Targeting this process has been shown to be a potential protective strategy. However, the intercellular communication in post-infarction angiogenesis remains unclear.

MicroRNAs (miRNAs), non-coding and conserved molecules, have been well-explored as biomarkers for the diagnosis or prognosis of coronary vascular diseases. Meanwhile, miRNAs are indispensable regulators of gene expression in various diseases including MI [5, 6]. In *vitro* and in vivo experiments, the knockdown of certain miRNAs has been shown to promote vascular growth and the functional recovery of damaged myocardium [7, 8]. Overall, exploring the mechanisms and therapeutic potential of miRNAs in promoting angiogenesis may contribute greatly to the treatment of MI.

Recently, several approaches have been developed to deliver miRNAs, and exosomes have been increasingly investigated as a delivery mechanism. Exosomes are small membrane micro vesicles produced by endocytosis. They mediate cross-talk between cells by transferring intracellular molecules, including enzymes, DNA, mRNA, and miRNAs [9]. Current research has demonstrated that exosomes participate in cardiac repair after ischemic injury by transferring miRNAs to regulate the crosstalk among endothelial cells, cardic cells and immune cells [10, 11]. Moreover, exosomes may represent a significant component of the paracrine effect for therapeutic angiogenesis [12, 13]. However, the impact of miRNAs originating from exosomes of myocardial infarction model on angiogenesis remains uncertain. In this study, we extracted serum exosomes and investigated differentially expressed miRNAs to determine the factors affecting angiogenesis in MI and identify additional effective therapeutic strategies.

Materials and methods

Establishment of AMI Rat Models

This study was supported by the Animal Care Committee of Dongzhimen Hospital, Beijing University of Chinese Medicine (No. 19 – 02). All animal studies were conducted in accordance with the Guidelines for the Care and Use of Laboratory Animals established by the Ministry of Science and Technology of the People's Republic of China. Specific pathogen-free (SPF) male Sprague–Dawley (SD) rats were obtained from Weitong Lihua Experimental Animal Technology Co., Ltd., Beijing, China (Certificate of Conformity: SCXK (JING) 2016-0006). All rats were housed in an SPF environment (Barrier Animal Laboratory of Dongzhimen Hospital, Beijing, China) with a light/dark cycle providing a circadian rhythm. MI models were randomly allocated and generated in rats weighing 200–250 g via ligation of the left anterior descending (LAD) coronary artery. Briefly, the rats were anesthetized with intraperitoneal injection of 1% sodium pentobarbital (50 mg/kg). The adequacy of anesthesia was confirmed by the absence of a withdrawal response to hind paw nociceptive stimulation. Anesthesia was maintained by supplying half dose pentobarbital i.p. as required when plantar reflex could be elicited. Body surface electrocardiogram (ECG) was monitored throughout the experiments by using standard limb leads (AD Instruments, Bella Vista, Australia). After endotracheal intubation, mechanically ventilate with an animal ventilator was necessary. An incision was made on the outer skin at the third and fourth ribs of the left chest. The LAD coronary artery was ligated approximately 2 mm below the arterial cone and the left atrial appendage [14]. The anterior wall of the myocardium was ischemic and whitening immediately. As shown in the electrocardiogram (ECG) in Fig. 1A, the ST segments of leads V1-V6, I, and aVL were significantly hunched upward immediately after the operation, indicating extensive anterior and high lateral left ventricular MI caused by occlusion of the anterior descending branch of the left coronary artery. On the second day after surgery, pathological Q-waves of thoracic lead, lead I and aVL were observed, which represented the presence of myocardial injury. Thus, the successful MI model was conducted (Table 1). The rats in sham operation group showed normal ECG since they were threaded without ligation. Each group contains eight rats. The thoracic incision was closed carefully.

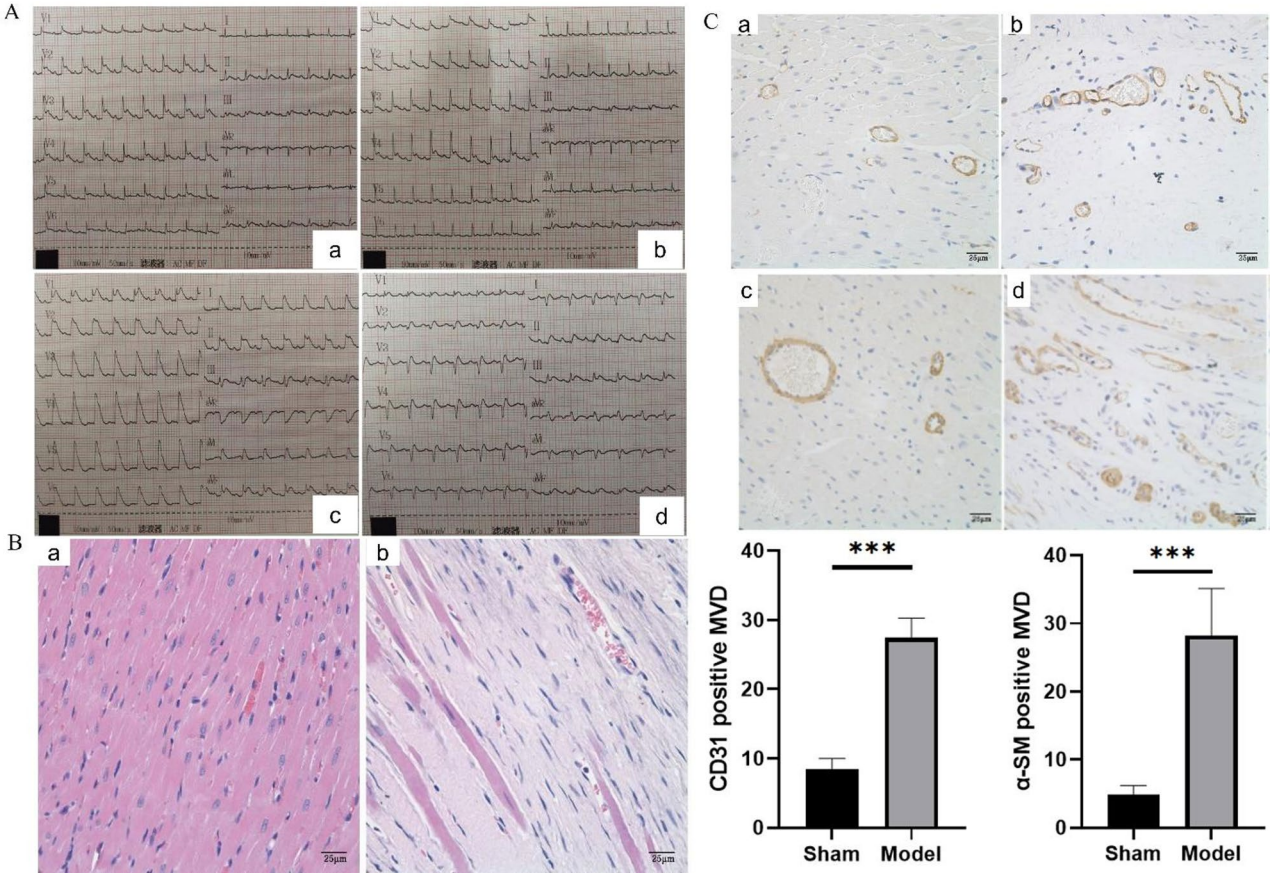

Fig. 1 Pathology in the sham and model groups. (A) ECG performance. a: Immediate postoperative ECG of rats in the control group; b: ECG of rats in the control group 24 h after the operation; c: immediate postoperative ECG of rats in the MI model group; d: ECG of rats in the MI model group 24 h after the operation. (B) Pathological changes in myocardial tissue in the sham group (a) or model group (b) (×400), $n = 8$, 4.82 ± 1.38 vs. 28.2 ± 6.94, $^{***}P < 0.001$, compared with the sham group. The nuclei were stained blue, and the cytoplasm was stained purple. (C) Comparison of the Microvascular density (MVD) between the sham and model groups. (a) CD31 in sham group, (b) CD31 in model group, c.α-SM in sham group, d.α-SM in model group. $n = 8$, 8.48 ± 1.50 vs. 27.43 ± 2.85, $P < 0.001$, power = 0.99; 4.82 ± 1.38 vs. 28.2 ± 6.94, $P < 0.001$, power = 0.99

Table 1 Timetable for ECG of MI after ligation in rats

	ECG performance	Pathological explanation
Day 1	Elevated ST segment of leads V1-V6, I, and aVL	Myocardial infarction involving extensive anterior and high lateral left ventricular
Day 2	Pathological Q-waves of thoracic lead, lead I and aVL	Myocardial injury

After awakening, the rats were placed back into the cage for intensive monitoring. The rats were anesthetized and euthanized after 28 days. Myocardial tissues were collected at the margin of the infarction. Subsequently, an additional intraperitoneal injection of an overdose of sodium pentobarbital (100–150 mg/kg) was administered to ensure that the animals reached deep anesthesia and were ultimately euthanized.

Hematoxylin–eosin (HE) Staining

Dehydrated, paraffin-embedded myocardial tissues were cut into 3-μm slices. The slices were dewaxed with xylene, hydrated with ethanol, and stained with HE (BLB-03 and YH-102, Beijing Kyushu Berlin Biotechnology Co. Ltd., China). After the dehydration and transparency steps, coverslips were placed sealed with neutral gum. Pathological changes in myocardial tissue were observed under an optical microscope (×400).

Immunohistochemistry

Heart slices (5 μm) were dewaxed in xylene and rehydrated in ethanol. Antigen retrieval was performed by boiling in 0.01 M citrate buffer. After eliminating endogenous peroxidase activity, the sections were successively incubated with goat serum blocking solution for 15 min at room temperature, anti-CD31 (1:2000, ab182981, Abcam) or anti-α-SM (1:5000, 14395-1-AP, Proteintech) overnight at 4 °C, and horseradish peroxidase-labeled goat anti-rabbit IgG. Finally, the sections were sealed with neutral gum and observed under an optical microscope after DAB (ZLI-9018, Beijing Zhongshan Jinqiao Biotechnology Co., LTD) color reaction and hematoxylin

counterstaining. Microvascular density (MVD) was used to indicate the CD31-positive and α-SM-positive regions. MVD within the infarct region was quantified at 400× magnification through enumeration of brown-stained endothelial cells and microvascular clusters. Vessels with luminal diameters exceeding 50 μm were omitted from analysis. The five regions with the highest capillary density were selected for microvessel counting as the microvessel density of one sample. Vessels with lumens larger than 50 μm were not included in the count.

Exosome extraction

Exosome isolation employs corresponding kits based on different sample types and detection requirements: For serum exosome isolation, the exoRNeasy Midi Kit (77144, QIAGEN) is used for flow cytometry analysis. The process involves pre-centrifugation, mixing with Buffer XBP for column binding, washing with Buffer XWP, secondary elution with Buffer XE, and centrifugation at 5,000 g to collect high-purity exosomes; ExoQuick™ Serum/Ascites Exosome Precipitation Kit (ExoQ5A-1, AMSbio) is used for transmission electron microscopy (TEM), where samples are obtained through exosome precipitation with ExoQuick reagent at 4 °C, resuspended in Buffer B, and eluted via column; for cell supernatant exosomes, YEASEN Exosome Extraction Kit (41208ES10, YEASEN) is employed. The procedure includes centrifugation at 3,000 g to remove debris, concentration by incubation with ECS reagent at 4 °C, pellet collection via centrifugation at 10,000 g, resuspension in PBS to eliminate impurities, and purification using an EPF column, ultimately yielding a high-purity exosome suspension.

Transmission electron microscopy (TEM)

The purified exosome suspensions were precipitated on copper grids and negatively stained with 2% uranyl acetate. TEM (Tecnai G2 spirit, FEI, America) was performed to determine the exosome morphology.

Nanoparticle tracking analysis (NTA)

The extracted exosomes were diluted in PBS. The size distribution and concentration of the exosomes were determined by a ZetaView PMX 110 particle matrix (Particle Metrix, Germany) under 405 nm emission light.

Flow cytometry

The serum samples were incubated with PE-labeled CD81 (CABT-48271HM, Creative Diagnostics) and FITC-labeled CD63 (ab108950, Abcam) for 30 min and detected by flow cytometry. Firstly, the unstained control was runed to set a threshold for autofluorescence, and then the labeled/stained samples were runed. The proportion of CD63 and CD81 was used to indicate the purity of the exosomes.

miRNA Sequencing

As has been mentioned above [15], five serum exosome samples were randomly selected from AMI and sham groups for miRNA sequencing. Total RNA extraction was performed, followed by 3' and 5' adapter ligation, reverse transcription to generate cDNA, and PCR amplification. Target microRNA fragments were separated via gel electrophoresis, with 147 nt and 157 nt bands excised, recovered, and purified. Qualified libraries were subjected to high-throughput sequencing. Raw sequencing data underwent adapter trimming, size selection (15–41 bp), Q20 quality filtering (≥ 80%), and removal of N-containing sequences to obtain clean reads. These reads were aligned to the reference genome and Rfam database for annotation and elimination of non-miRNA and repetitive sequences. Novel miRNAs were identified using Mirdeep2, and expression levels were quantified as transcript per million (TPM). Differential expression analysis identified candidate miRNAs for target prediction, followed by bioinformatics analysis.

Bioinformatics analysis

The targets of differentially expressed miRNAs were anticipated utilizing Miranda software, under the specified parameter settings: $S \geq 150$, $\Delta G \leq -30$ kcal/mol, and requiring strict 5' seed pairing. The Gene Ontology (GO) and Kyoto Encyclopedia of Genes and Genomes (KEGG) pathway enrichment analysis were performed to elucidate the biological processes and pathways controlled by miRNAs using R based on the hypergeometric distribution. The protein-protein interaction network (PPI network) analysis was performed on the corresponding proteins of signal pathway through STRING website (https://string-db.org/) and Cytoscape software.

The rno-miR-484 and R-VEGFA-3'UTR sequences were queried through the NCBI (https://www.ncbi.nlm.nih.gov/) and miRBase (https://www.mirbase.org/) databases to explore the binding relationship between miR-484 and VEGFA, which was subsequently predicted by TargetScan 7.2 (https://www.targetscan.org/mmu_72/).

MiRNAs expression analysis

Total RNA in myocardial tissues, human umbilical vein endothelial cells (HUVECs), H9c2 cells, and exosomes was extracted using the mirVanaTM RNA Isolation Kit (AM1561, Applied Biosystems, USA). The miScript II Reverse Transcription Kit and QuantiFast® SYBR® Green PCR Master Mix (Qiagen, Germany) were used for the reverse transcription and real-time PCR separately. The reactions were incubated under conditions according to manufacturer's instructions. Using 5S as a template, the expression of the miRNAs was normalized, and the expression of VEGFA was compared, with GAPDH serving as an internal reference. The primer pairs used were

as follows: GAPDH, F5'-GGGTGTGAACCATGAGAAG T-3' and R5'-GACTGTGGTCATGAGTCCT-3'; VEGFA, F5'-CTGTCTTGGGTGCATTGGAG-3' and R5'-ACCA GGGTCTCGATTGGATG-3'. The relative gene expression was conducted with $2^{-\Delta\Delta CT}$ method. The sequences of the microRNA-specific primers used are shown in Table 2.

Dual-luciferase reporter assay

HUVECs were cultured in DMEM containing wild-type and mutated miR-484 binding sites in the 3′UTR of VEGFA and HiPerFect Transfection Reagent. The direct interaction between miR-484 and VEGFA was assessed using a dual-luciferase reporter system. Wild-type (r-Vegfa-3UTR-wt) or mutant (r-Vegfa-3UTR-mu) fragments of the rat Vegfa 3′UTR were cloned into the pmiGLO vector. 293T cells were seeded in 96-well plates and co-transfected with either plasmid (0.16 μg) and rno-miR-484 mimic or negative control (5 pmol) using a liposome-based reagent. After 48 h of transfection, the assays were conducted using a Dual-Luciferase System Assay kit (Promega, Germany). The Firefly luciferase value was used as the internal reference, and the Renilla luciferase value was measured and recorded. The ratio of the Renilla and Firefly luciferase values was used to determine the binding relationship between miR-484 and VEGFA. Further, qRT-PCR was used to detect the changes of VEGFA mRNA expression in HUVEC after miR-484 overexpression and expression suppressions.

Cell culture, passage and hypoxic culture

Rat cardiomyocytes (H9c2s) were derived from rat embryo cardiomyocyte cell lines and purchased from the National Experimental Cell Resource Sharing Service Platform of the China Academy of Medical Sciences (No. 1101RAT-PUMC000219). HUVECs were obtained from Shanghai Zhongqiao Xinzhou Biology Company (Shanghai, China). H9c2 cells were cultured in high-sugar DMEM (Solarbio, Beijing, China) with 5% fetal bovine serum (FBS) (Gibco, Shanghai, China) and 1% penicillin/streptomycin (p/s) at 37 °C with 95% O_2 and 5% CO_2 (normal oxygen concentration). HUVECs were cultured in endothelial cell medium supplemented with 5% FBS and 1% p/st at 37 °C with 95% O_2 and 5% CO_2. When the cells reached 80%-90% confluence, proceed with passaging using 1 mL of 0.25% trypsin solution. Upon observing that the majority of cells appear as single cells under the microscope, 3 mL of complete culture medium was added to terminate the digestion. After centrifugation and resuspension of the cells, they were transferred to a new flask at a ratio of 1:3 and incubated at 37 °C in a 5% CO_2 incubator. For hypoxic culture, H9c2s and HUVECs were cultured in their basic medium in a standard incubator (RS Biotech, MiniGalaxy R, England) comprising 94% N_2, 5% CO_2, and 1% O_2 (hypoxia-H9c2s) [16, 17]. After 24 h, the culture supernatant of H9c2 or hypoxia-H9c2 cells was collected and centrifuged to obtain exosomes.

Table 2 Primer sequences

Gene Symbol	Forward primer (5′→3′)
novel1073_mature	CGGTATTGGTTGGATGAGGT
novel539_mature	GTTCCGGTCTGTGCCTCCA
novel921_mature	CGGATCTTGGTAGAACCTCCA
novel951_mature	GGGTCAGCGGCTGGGGTG
rno-miR-181d-5p	AACATTCATTGTTGTCGGTGGGT
rno-miR-484	GCTCAGTCCCCTCCCGATAA
5 S	GGAGACCGCCTGGGAATA

Coculture of HUVECs with exosomes

HUVECs were cocultured with exosomes derived from H9c2 cells under hypoxic or normoxic conditions as follows. Based on CCK-8 results, the optimal exosome concentration was determined. HUVECs were divided into four groups: normoxia, hypoxia, EXO-M (hypoxic H9c2-derived exosomes), and EXO-C (normoxic H9c2-derived exosomes). When cell confluence reached > 70%, the medium was replaced with 0.5% FBS ECM for synchronization. After 24 h, the normoxia group was maintained in xeno-free and serum-free exosome-specific medium (UR51102, Umibio) under normal culture conditions. Meanwhile, the hypoxia, EXO-M, and EXO-C groups were placed in a hypoxic incubator for 24 h. The EXO-M and EXO-C groups were treated with exosome-specific medium containing the corresponding optimal concentration of exosomes.

Confocal imaging

Laser scanning confocal microscopy was used to observe interactions between the exosomes and HUVECs. For fluorescence staining, exosomes derived from H9c2 and hypoxia-H9c2 culture supernatants were incubated with the green fluorescent dye PKH26 (Umibio, Shanghai, China) at room temperature for 10 min. Then, HUVECs were cultured with 10 μg/ml H9c2-exos (Exo-C group) or hypoxia-exposed H9c2-exos (Exo-M group) at 37 °C for 24 h with 5% CO_2. Subsequently, the samples were fixed with 4% paraformaldehyde for 15 min, and the cell nuclei were stained with DAPI (BBI, Hong Kong, China). The samples were observed under laser scanning confocal microscopy (TCS SP8, Leica, Germany).

Knockdown (KD) and overexpression (OE) of miR-484

miR-484 was knocked down or overexpressed in HUVECs to determine the impact of this miRNA on the proliferation, migration, and tube formation capacities of these cells. Briefly, HUVECs was evenly seeded with 5,000 cells per well in 96-well plates. After 24 h, HUVECs were

cultured in serum-free basic ECM (Shanghai Zhongqiao Xinzhou Biology Company, 1001 China) supplemented with HiPerFect Transfection Reagent (Qiagen, Germany), miR-484 mimics, miR-484 mimics NC, miR-484 inhibitor, or miR-484 inhibitor NC for 6 h and cultured in medium with 5% FBS for 48 h. The final concentration of the miR-484 mimics/mimics NC working solution was 200 nM, while that of the Mir-484 inhibitor/inhibitor NC working solution was 400 nM. The expression of miR-484 in HUVECs was certificated by qRT−PCR.

Cellular proliferation assay

The experiment was conducted using a Cell Counting Kit-8 (CCK-8) Assay Kit (CK04-1, Japan Tongren Institute of Chemistry). Briefly, HUVECs was evenly seeded with 5000 cells per well in 96-well plates. the supernatant was discarded, and the cells were cultured in basic ECM supplemented with CCK-8 solution for 3 h. The optical density (OD) of each sample at 450 nm was measured using a spectrophotometer (Thermo Scientific, Varioskan Flash, USA).

Scratch wound assay

HUVECs was evenly seeded with 12.5×10^4 cells per well in 6-well plates. A scratch wound was manually made with a sterile 200-μl pipette tip. Images of the wound area were taken using an inverted microscope (Olympuso, MT-2, Japan) after culturing with basic ECM medium (Cat. #:1001, Shanghai Zhongqiao Xinzhou Bio-Technology Co., Ltd.) for 0 h and 12 h. Migration was analyzed using ImageJ software. Each condition was assessed in at least triplicate. The mobility (%) was calculated as Mobility (%) = $(A_0\text{-}A_x)/A0 \times 100\%$, in which A0 represents the initial wound area and A_x represents the residual area after 12 h.

Tube formation assay

HUVECs was evenly seeded with 2×10^4 cells per well in 96-well plates. The 96-well culture plates were precoated with liquid Matrigel (Solarbio, M8370, China) at 37 °C for 30 min. The HUVECs were then visualized, and tube formation was quantified using an inverted microscope (Olympuso, MT-2, Japan) after culturing with basic ECM medium for 6 h. Tube numbers and branch points were statistically analyzed using ImageJ software. Each condition was assessed at least three times.

Western blot

Tissue and cell samples were first lysed for 5 min at room temperature in an SDS lysis buffer. Then, the supernatant of lysate was collected via centrifugation. After the amount of protein in each sample was quantified, an equal amount of protein from each sample was boiled and then resolved on a 15% SDS-PAGE gel. In the next step, the resolved protein was transferred onto nitrocellulose membranes and incubated in sequence with VEGFA (ab39250, abcam) primary antibodies and appropriate secondary antibodies. After being developed using enhanced chemiluminescence reagents, the protein bands were imaged and analyzed using GAPDH as the internal standard to calculate the relative expression.

Statistical methods

SPSS software package version 20.0 was used for the statistical analysis. Pass 11.0 was used for the power analysis. During the experiment, group allocation, measurement and data analysis were all conducted by independent researchers respectively to avoid potential bias. The results are expressed as the mean ± standard deviation ($\bar{x} \pm s$). For normally distributed data, One-way analysis of variance (ANOVA) was performed and the least significant difference (LSD) test was used for pairwise comparisons between groups. Nonparametric tests of independent samples were used for data that did not follow a normal distribution. $P < 0.05$ indicated a significant difference.

Results

Increased myocardial angiogenesis in the MI model group

Pathological staining can directly reveal morphological changes in myocardial tissue. Cardiomyocytes with a complete structure, uniform shape, clear nucleus, and uniform cytoplasm were observed in the sham group. The myocardial muscle bundles were tightly and neatly arranged. In contrast, the myocardial tissue structure was destroyed in the model group and was replaced with large areas of fibrotic scars (Fig. 1B), which increased myocardial stiffness and impaired cardiac systolic and diastolic functions. Notably, the MVD in the model group was significantly greater compared with that in the sham group (8.48 ± 1.50 vs. 27.43 ± 2.85, $P < 0.001$, power = 0.99; 4.82 ± 1.38 vs. 28.2 ± 6.94, $P < 0.001$, power = 0.99) (Figs. 1C).

Extraction and identification of exosomes

Exosomes were extracted from serum of sham and MI model rats. The typical spherical or saucer-like structure of exosomes was observed by TEM (Fig. 2A) with a diameter distribution ranging from 40 nm to 160 nm, which was revealed by NanoSight analysis (Fig. 2B). The diameter of the peak was 134.2 nm with a concentration of 1.8×10^7 particles/mL. By means of flow cytometry measurement, the experimental results clearly demonstrated the particle size distribution of the samples. Firstly, the calibration of the instrument is realized based on the standardized microspheres with known particle size, and the particle size region is effectively delineated. With 100 nm as the boundary, it was found that the majority of

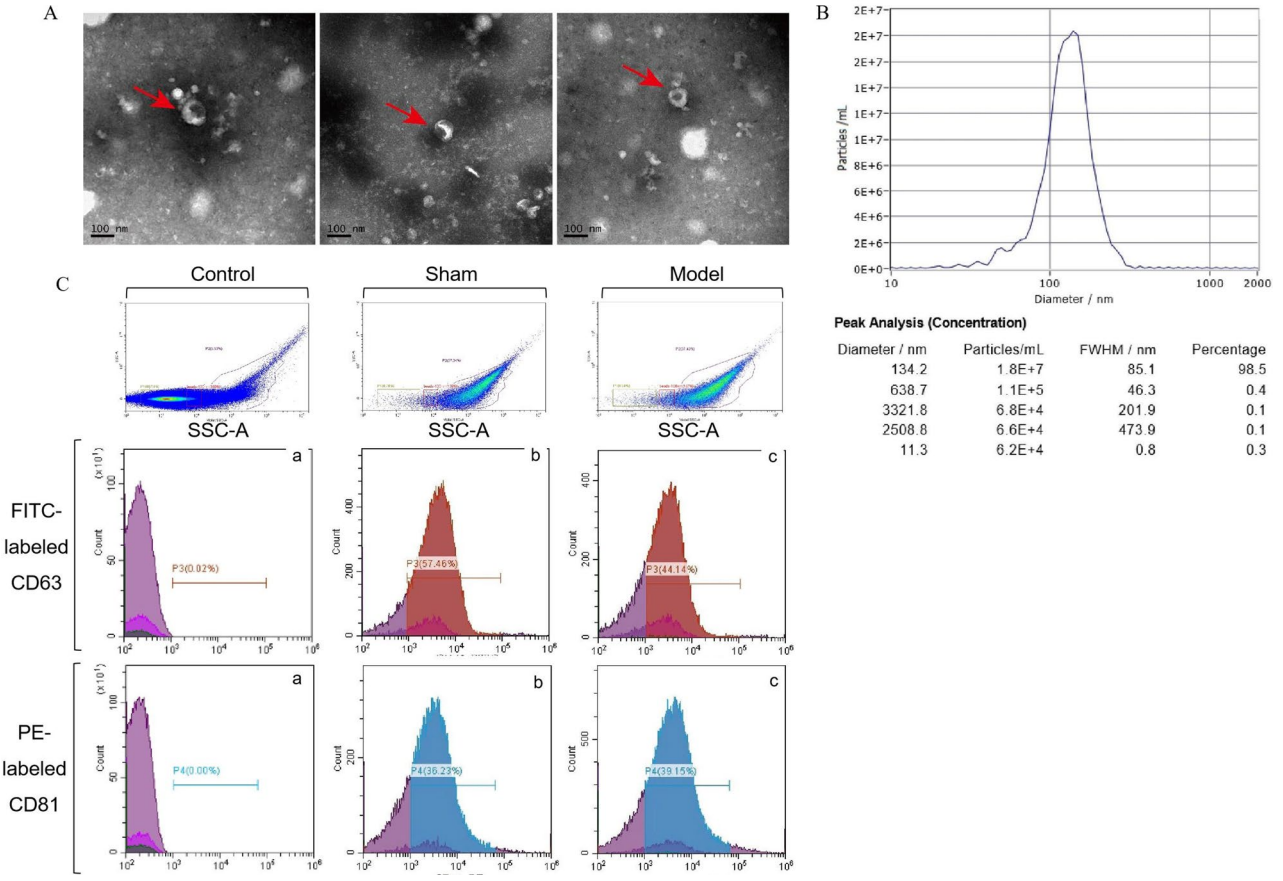

Fig. 2 Characterization of exosomes. (A) TEM of exosomes. The red arrow in the figure indicates exosomes. (B) NTA detection of exosomal particle size. (C) Detection of the exosomal marker proteins CD63 (a: Unstained control; b: shamed group; c: model group) and CD81 (a: Unstained control; b: shamed group; c: model group) by flow cytometry

particles in the sham operation and model groups had a size larger than 100 nm. We selected the particles above 100 nm for observing the proportion. In quick succession, the positive expression of CD63 (57.46% or 44.14%), and CD81 (36.23% or 39.15%) in exosomes derived from sham- or model-serum, separately, were further confirmed by flow cytometry assay (Fig. 2C). On the whole, these results demonstrated that the micro-vesicles isolated from the serum were exosomes.

Bioinformatics analysis and verification of differentially expressed miRNAs

Differentiated exosome miRNA expression profiles between the sham and model groups were detected to identify the candidate miRNAs that may play a role in exosomes-mediating angiogenesis. Twenty-two differentially expressed miRNAs were screened (FC ≥ 2.0, $P \leq 0.05$), including novel1007_mature, novel10_star, novel1147_mature> novel1170_mature, novel208_mature, novel238_mature, novel335_mature, novel407_mature, novel539_mature, novel65_mature, novel898_mature> novel1221_mature, novel921_mature, novel951_mature, rno-miR-484, rno-miR-615, rno-miR-676, novel1073_mature, novel130_mature, novel311_mature, novel738_mature, novel867_mature> novel928_mature, novel903_mature, rno-miR-181d-5p (Table 3). Fifteen of these genes were downregulated, and seven were upregulated, as shown in the heatmap (Fig. 3A). The different longitudinal sample clusters clearly distinguished the two groups. MiRNAs with similar biological functions were gathered in the horizontal sample clustering tree. The miRNAs with upregulated expression are indicated in red, and those with downregulated expression are indicated in blue; the brighter the color, the more significant the difference.

Total of 7002 genes were obtained as the target genes of 22 differentially expressed miRNAs, predicting by miRanda database. GO analysis of common target genes revealed the functions of differentially expressed miRNAs, including cellular components, molecular functions, and biological processes (Fig. 3B). Enrichment statistical analyses were conducted for the target genes in each GO category. The potential signaling pathways targeted by the miRNAs were performed by KEGG

Table 3 Differentially expressed miRNA in serum exosomes from MI model group and sham group

miRNA_id	*P* value	Regulation
novel1073_mature	0.045276594	Down
novel10_star	0.00349428	Down
novel1147_mature> novel1170_mature	0.0179458	Down
novel208_mature	0.025475967	Down
novel238_mature	0.04887685	Down
novel335_mature	0.034917366	Down
novel407_mature	0.020025425	Down
novel539_mature	0.001238356	Down
novel65_mature	0.01751887	Down
novel898_mature> novel1221_mature	0.000562578	Down
novel921_mature	0.001914019	Down
novel951_mature	0.003663281	Down
rno-miR-484	0.008585866	Down
rno-miR-615	0.013813453	Down
rno-miR-676	0.023315362	Down
novel1073_mature	0.001724784	UP
novel130_mature	0.018611731	UP
novel311_mature	0.034303457	UP
novel738_mature	0.002396518	UP
novel867_mature> novel928_mature	0.025759137	UP
novel903_mature	0.019018713	UP
rno-miR-181d-5p	0.026820228	UP

enrichment analysis. As shown in Figs. 3C and 113 signaling pathways, including insulin secretion, amphetamine addiction, CAMP signaling, oxytocin signaling, calcium signaling, GnRH signaling, arrhythmogenic right ventricular cardiomyopathy (ARVC), long-term potentiation, adherents' junction, axon guidance, and ECM-receptor interaction, were identified ($P<0.05$) (Fig. 3C).

miRNA expression in serum exosomes of MI model group and sham group

Subsequently, we validated these candidate molecules in an independent serum sample cohort using more specific and sensitive RT-qPCR technology. Ultimately, we successfully confirmed the stable presence of 8 novel miRNAs in the serum exosomes, while the remaining candidates were either too low in abundance or could not be reproducibly detected in the serum. Among them, only 5 miRNAs were amplified by q-RT PCR with a single peak, and the amplification rate was stable. The expression trends in serum exosomes between the sham and MI model groups were consistent with the chip results (Fig. 4A and C).

miR-484 targets calcium signaling pathway

Among 5 miRNAs, only miR-484 has been previously validated to be associated with pathological angiogenesis in tumors [18, 19]. In this study, miR-484 declined in serum and cardiac tissue after MI, coinciding with an increase in neovascularization within the infarcted myocardium. This pattern was significantly observed during the chronic phase (day 28), whereas it is not obvious during the acute phase (day 1) (Fig. S1, 1 C), suggesting a potential functional role. Therefore, miR-484 was preferred to further evaluate the biological functions. The results showed that miR-484 predicted 357 target genes. The GO function analysis indicated that miR-484 target genes affected 14 cell components, regulated 19 molecular functions and participated in 27 biological processes (Fig. 4B). Enrichment analysis of miR-484 performed 4 KEGG signaling pathways, including dilated cardiomyopathy, arrhythmogenic right ventricular cardiomyopathy, hypertrophic cardiomyopathy and calcium signaling pathway (Table 4), among which calcium signaling pathway was the most closely related with angiogenesis. PPI analysis showed that CACNA1E, CACNA1D, RYR2, ATP2A2 have interactions (Fig. 4C).

miR-484 expression increased in HUVECs after culture with exosomes from hypoxia-exposed H9c2 cells

Given the miRNA expression profile, we selected miR-484 for further investigation. Exosomes were extracted and cultured with HUVECs for 24 h to determine the exosomal uptake capacity of HUVECs. Exosomes labeled with PKH26 were found to overlap with HUVECs labeled with DAPI under the confocal microscope, suggesting that exosomes were successfully internalized by HUVECs (Fig. 5A). qRT−PCR was performed to determine the expression of miR-484. miR-484 expression was downregulated in hypoxic H9c2 cells compared with that in H9c2 cells (0.550 ± 0.126 vs. 1.013 ± 0.201, $P=0.03$, power = 0.76) (Fig. 5B). In contrast, significantly upregulated miR-484 expression was observed in exosomes derived from hypoxic H9c2 cells (1.019 ± 0.223 vs. 3.860 ± 1.503, $P=0.01$, power = 0.73) (Fig. 5C). Compared with that in hypoxic HUVECs, the level of miR-484 in hypoxic HUVECs cultured with exosomes stemmed from hypoxic H9c2 cells was also more abundant (1.007 ± 0.147 vs. 1.274 ± 0.084, $P=0.01$, power = 0.75) (Fig. 5D).

miR-484 inhibits the proliferation, migration, and tube formation of HUVECs

miR-484 in HUVECs was overexpressed or knocked down, transfecting with miR-484 mimics or inhibitors respectively (Figs. 6A). The proliferation rate, migration area, and tube formation capacity of HUVECs over-expressed with miR-484 were significantly reduced (0.485 ± 0.011 vs. 0.534 ± 0.039, $P=0.04$, power = 0.85; 10806475.68 ± 866937.12 vs. 15713666.85 ± 810625.50, $P<0.001$, power = 0.99; 84264.70 ± 6782.77 vs. 384021.23 ± 43246.07, $P<0.001$, power = 0.99), while the down-regulation of miRNA in HUVECs showed the opposite effect (0.604 ± 0.083 vs. 0.491 ± 0.039, $P<0.001$, power = 0.89; 17454520.16 ± 86849.58 vs.

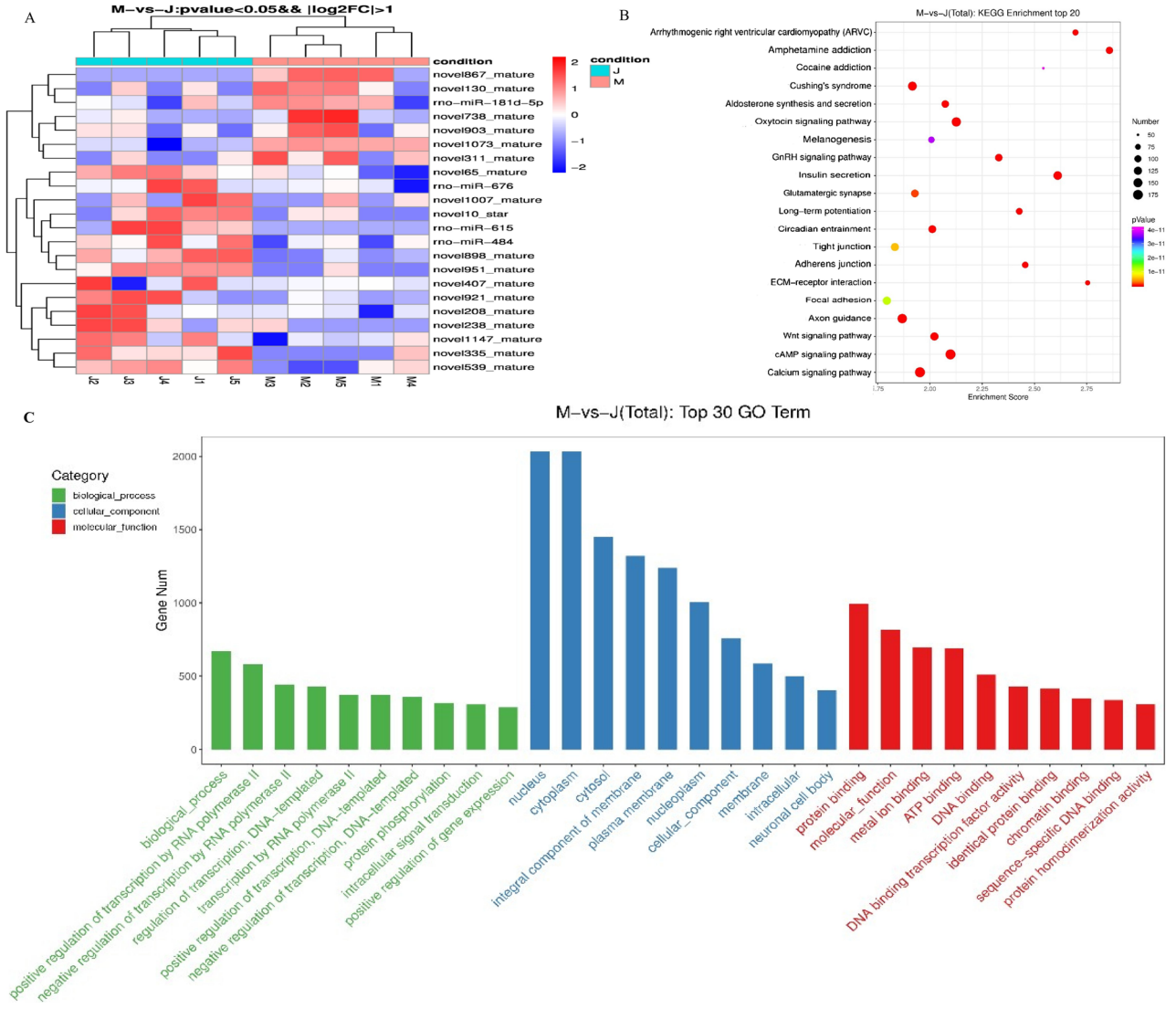

Fig. 3 Bioinformatics analysis of differentially expressed miRNAs between the sham and model groups. **A** Heatmap of exosomal miRNAs in the serum of the model and sham groups. The right side of the heatmap shows the name of the exosomal miRNA probe, and the bottom side shows the name of the sample. The color scale represents the change in gene expression from relatively low (blue) to relatively high (red). **B** KEGG signaling pathway enrichment analysis of the target genes of the differentially expressed miRNAs. The vertical axis represents the KEGG pathway, and the horizontal axis represents the gene ratio. The greater the gene ratio is, the greater the degree of enrichment is. **C** GO analysis of target genes of differentially expressed miRNAs

14963398.91 ± 737084.79, $P = 0.01$, power = 0.85; 458707.90 ± 21952.36 vs. 369072.41 ± 39389.14, $P = 0.02$, power = 0.90) (Figs. 6B, C and D). Overall, miR-484 may play an anti-angiogenic role manifested by inhibiting the proliferation, migration, and vascular formation of HUVECs.

miR-484 directly targets VEGFA

VEGF is the most specific cell growth factor known to promote angiogenesis, and VEGFA is the main form of this factor. A literature review revealed that miR-484 is closely related to angiogenesis. Bioinformatics analyses were conducted to investigate the regulatory relationship between miR-484 and VEGFA. VEGFA was found to contain two putative binding sites for miR-484 in the 3′UTR (Figs. 7A, B). The luciferase reporter assay revealed that the relative luciferase activity was decreased in HUVECs carrying the wild-type 3′UTR of VEGFA compared with those containing the mutant 3′UTR (0.636 ± 0.026 vs. 0.743 ± 0.015, $P < 0.001$, power = 0.99) (Fig. 7C), suggesting that miR-484 could directly target VEGFA. Furthermore, overexpression or knockdown of miR-484 reduced or elevated VEGFA mRNA and protein levels in HUVECs, separately (0.494 ± 0.113 vs. 0.963 ± 0.319, $P = 0.06$, power = 0.38; 1.358 ± 0.203 vs. 0.687 ± 0.072, $P = 0.008$, power = 0.38) (Fig. 7D and E). These results suggest that the effect of miR-484 carried by exosomes on angiogenesis might be regulated through

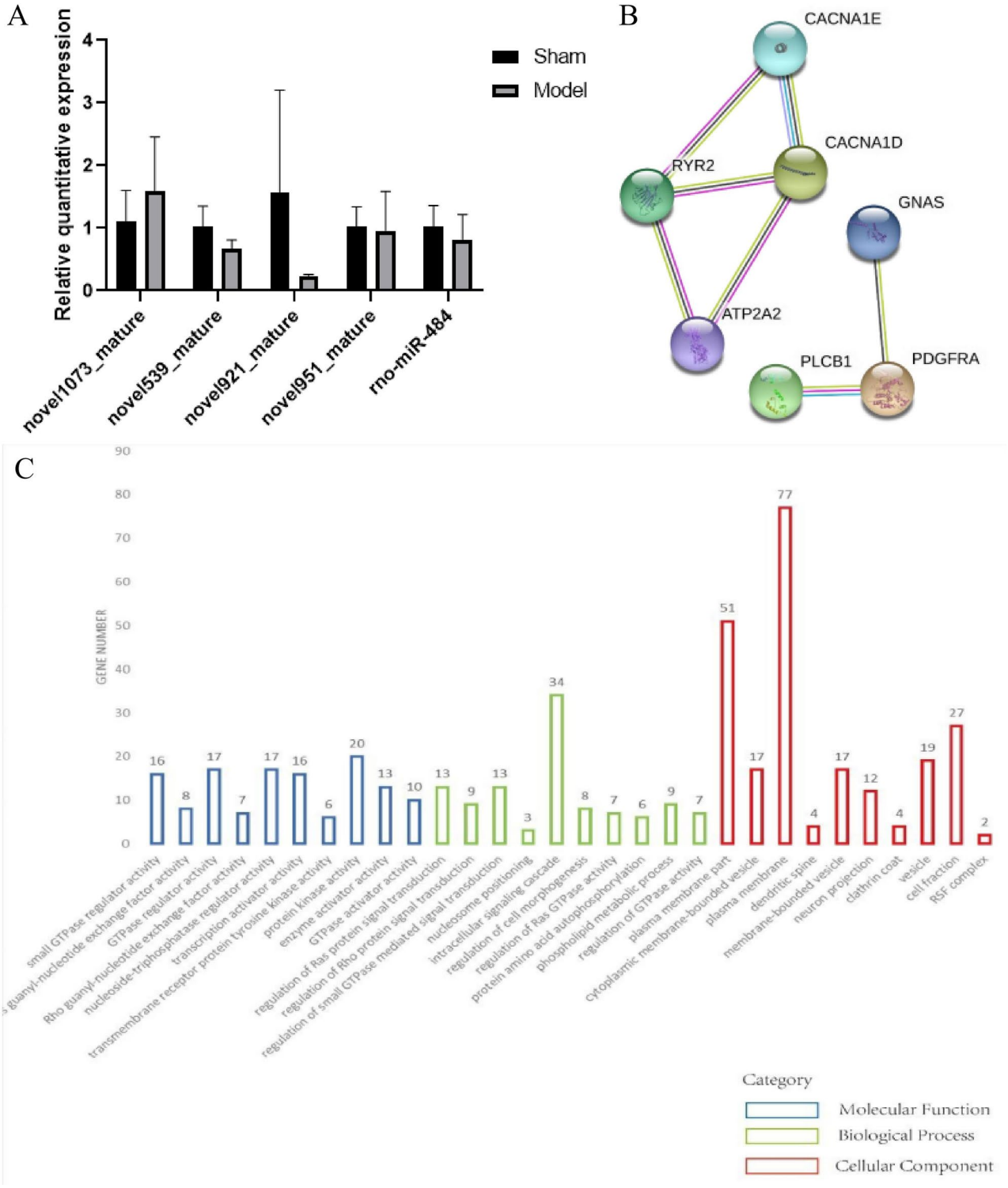

Fig. 4 Differential exosomes miRNAs expression in MI rat serum and bioinformatics analysis of miR-484. **A** The relative expression of differentially expressed miRNAs in serum exosomes between the sham and MI model groups. **B** GO enrichment analysis of miR-484 target genes. The vertical axis represented GO function entries, while the horizontal axis represented the three parts of GO, namely, Biological Process (BP), Cellular Component (CC), and Molecular Function (MF). The top ten items in each section were listed. **C** PPI analysis of the corresponding proteins of miR-484 target genes in calcium signaling pathway

Table 4 Enrichment analysis of the KEGG signaling pathway for target genes of miR-484

KEGG Pathway terms	*P* value	Genes
hsa05414: Dilated cardiomyopathy	0.004135	ITGA9, ATP2A2, RYR2, GNAS, ITGA4, CACNA1D, CACNA2D2
hsa05412: Arrhythmogenic right ventricular cardiomyopathy (ARVC)	0.008457	ITGA9, ATP2A2, RYR2, ITGA4, CACNA1D, CACNA2D2
hsa05410: Hypertrophic cardiomyopathy (HCM)	0.013363	ITGA9, ATP2A2, RYR2, ITGA4, CACNA1D, CACNA2D2
hsa04020: Calcium signaling pathway	0.026982	ATP2A2, SPHK2, PDGFRA, RYR2, GNAS, CACNA1E, PLCB1, CACNA1D

VEGFA signaling pathway, which was further validated by the supplementary assay (Figure S2).

Discussion

Previous studies have been conducted on the functions of exosomes and exosome-carried intracellular cargoes in various processes [20]. For example, miRNAs are stably transported to the target regions in which they play biological roles [21] in processes such as angiogenesis by regulating related factors [22]. In rats with ischemic injury, myocardial cells reportedly release cell-dependent exosomes in the blood circulation [23]. Thus, in this study, we isolated exosomes from the serum of MI model rats. To further determine the mechanism underlying the effect of MI-associated exosomes on angiogenesis, a microarray assay was performed to investigate the functions of miRNAs. After a literature review, among several candidate miRNAs, miR-484 attracted our attention. The exosomes were hypothesized to affect angiogenesis by regulating miR-484 in vivo after qRT−PCR validated the miRNA chip screening results.

Previous research has identified differential expression of miR-484 as a potential regulator of angiogenesis, particularly in oncological contexts [24]. Nonetheless, studies focusing on ischemic heart disease remain limited. Existing data suggest that, compared to healthy controls, circulating miR-484 levels in patients decline on days 1 and 7 following MI, though these changes are not statistically significant [25]. In a rat MI/reperfusion (MI/R) model, myocardial downregulation of miR-484 mitigated cardiomyocyte apoptosis within ischemic regions [26]. In our investigation, serum and ischemic tissue levels of miR-484 in rats post-MI displayed a decreasing trend on day 1, without reaching significance, concurrent with an upward trend in angiogenic markers CD31 and α-SMA. By day 28, miR-484 expression in serum and ischemic tissues significantly reduced, accompanied by a notable elevation of CD31 and α-SMA in ischemic regions. These findings imply that miR-484 may inversely regulate angiogenesis during MI progression, with its effects becoming more pronounced in the chronic phase. The precise mechanisms underlying this regulatory relationship, however, warrant further elucidation.

Calcium ion channels play a critical role in endothelial cell function and angiogenesis [27, 28]. These channels regulate calcium signaling, which is essential for endothelial cell migration, proliferation, and tube formation—key processes in angiogenesis. In the context of MI, calcium signaling is activated by VEGFA, and miR-484 may modulate this pathway. MiR-484's dysregulation could disrupt calcium signaling, thereby impairing angiogenesis and hindering myocardial repair. This study highlights the potential of miR-484 to target key calcium channels, particularly RYR2 and CACNA1D, which are implicated in the vascular repair process post-MI. Targeting miR-484 in these pathways could provide therapeutic benefits by promoting angiogenesis and enhancing myocardial recovery after ischemic injury.

Circulating miRNAs are derived from many cell types. Myocardial cell miRNAs are loaded into exosomes after AMI and mediate functional crosstalk between the ischemic heart and vascular endothelium.The results exhibited that miR-484 was downregulated in H9c2 cells and significantly increased in secreted exosomes after hypoxic culture. PKH26-labeled exosomes were found to be absorbed by HUVECs by confocal microscopy. Compared with that in HUVECs treated with hypoxia alone, the expression level of miR-484 in HUVECs co-incubated with exosomes derived from hypoxic H9c2 cells was significantly greater. These results suggest that hypoxia stimulates the sorting of miR-484 into myocardial exosomes, which then play a role in HUVECs through intercellular transmission.

A study by LI [24] suggested that miR-484 might inhibit angiogenesis in gastric cancer tissue. In subsequent experiments, the overexpression of miR-484 inhibited HUVEC proliferation and tube formation, whereas the knockdown of miR-484 had the opposite effect on angiogenesis, consistent with the results of previous studies. Moreover, miR-484 has been reported to be associated with angiogenesis in endothelial dysfunction in ovarian cancer [18]. Targeted delivery of miR-484 through exosomes promoted the normalization of blood vessels and sensitivity to chemotherapy, ultimately prolonging the survival time of mice with ovarian cancer [18]. Together, these observations revealed the importance of miR-484 in angiogenesis in various diseases and the possibility of delivering miR-484 through exosomes to treat MI.

It is noteworthy that the differential expression of miR-484 observed between in vitro and in vivo models can be attributed to distinct biological contexts. In the complex in vivo microenvironment, the downregulation of serum miR-484 results from a dynamic equilibrium between hypoxia-induced secretion, ischemic cell uptake, and

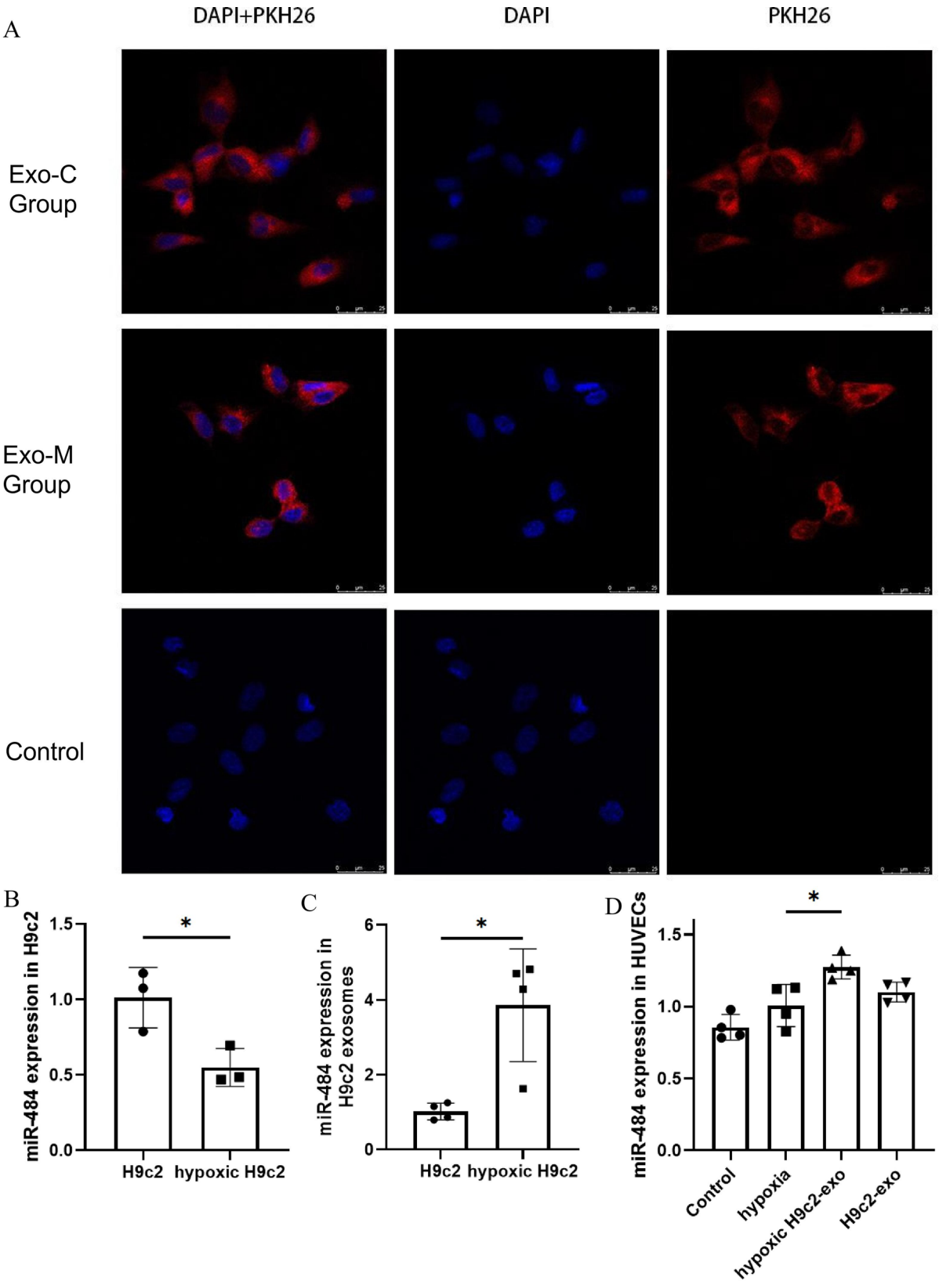

Fig. 5 (See legend on next page.)

(See figure on previous page.)

Fig. 5 The expression of miR-484 in HUVECs increased after culture with exosomes from hypoxia-exposed H9c2 cells. **A** Exosomes were internalized by HUVECs. Blue represents nuclei stained with DAPI, and red represents exosomes stained with PKH26. **B** Decreased miR-484 expression in hypoxic H9c2 cells. $n=3$, 0.550 ± 0.126 vs. 1.013 ± 0.201, $^{*}P=0.03$, compared with H9c2 cells. **C** Increased miR-484 expression in exosomes derived from hypoxic H9c2 cells. $n=4$, 1.019 ± 0.223 vs. 3.860 ± 1.503, $^{*}P=0.01$, compared with H9c2-exos. **D** Changes in the expression of miR-484 in HUVECs cultured with exosomes from different cells. $n=4$, 1.007 ± 0.147 vs. 1.274 ± 0.084, $^{*}P=0.01$, compared with hypoxia; the values are the means ± SDs

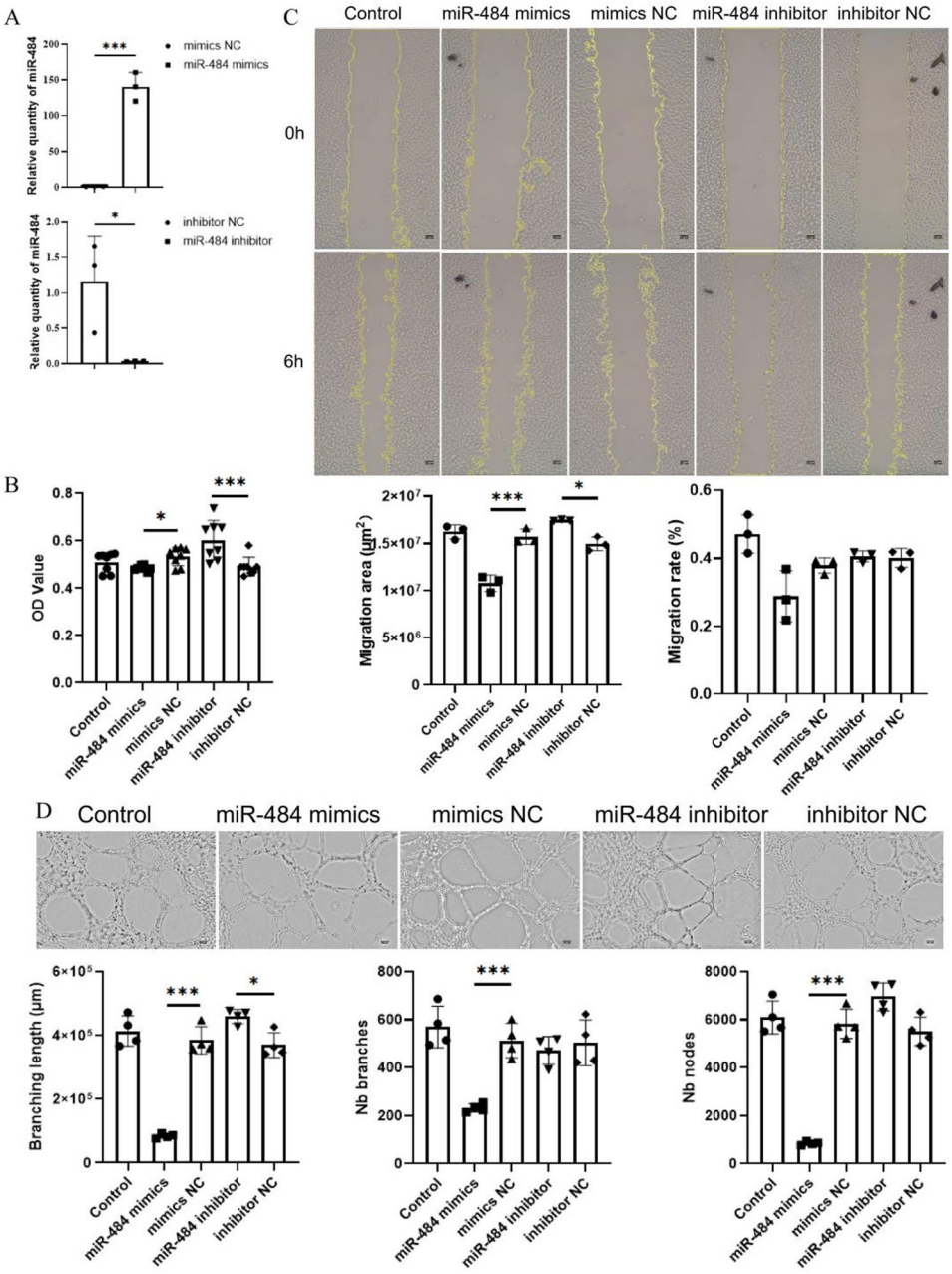

Fig. 6 miR-484 inhibits the proliferation, migration, and tube formation of HUVECs. **A** The expression of miR-484 in HUVEC after transfecting with miR-484 mimics or inhibitors. $n=3$, 1.003 ± 0.092 vs. 140.341 ± 20.068, $^{***}P<0.001$, compared with mimics NC; 1.158 ± 0.639 vs. 0.033 ± 0.004, $^{*}P=0.04$, compared with inhibitor NC. **B** Proliferation of HUVECs transfected with the miR-484 mimic or inhibitor. $n=8$, 0.485 ± 0.011 vs. 0.534 ± 0.039, $^{*}P=0.04$, compared with mimics NC; 0.604 ± 0.083 vs. 0.491 ± 0.039, $^{***}P<0.001$, compared with inhibitor NC. **C** Migration of HUVECs transfected with the miR-484 mimic or inhibitor. $n=3$, 10806475.68 ± 866937.12 vs. 15713666.85 ± 810,625, $^{***}P<0.001$, compared with mimics NC; 17454520.16 ± 86849.58 vs. 14963398.91 ± 737084.79, $^{*}P=0.01$, compared with inhibitor NC. **D** Tube formation of HUVECs transfected with the miR-484 mimic or inhibitor. $n=4$, 84264.70 ± 6782.77 vs. 384021.23 ± 43246.07, $^{***}P<0.001$, compared with mimics NC; 458707.90 ± 21952.36 vs. 369072.41 ± 39389.14, $^{*}P=0.02$, compared with inhibitor NC. Values are the means ± SDs

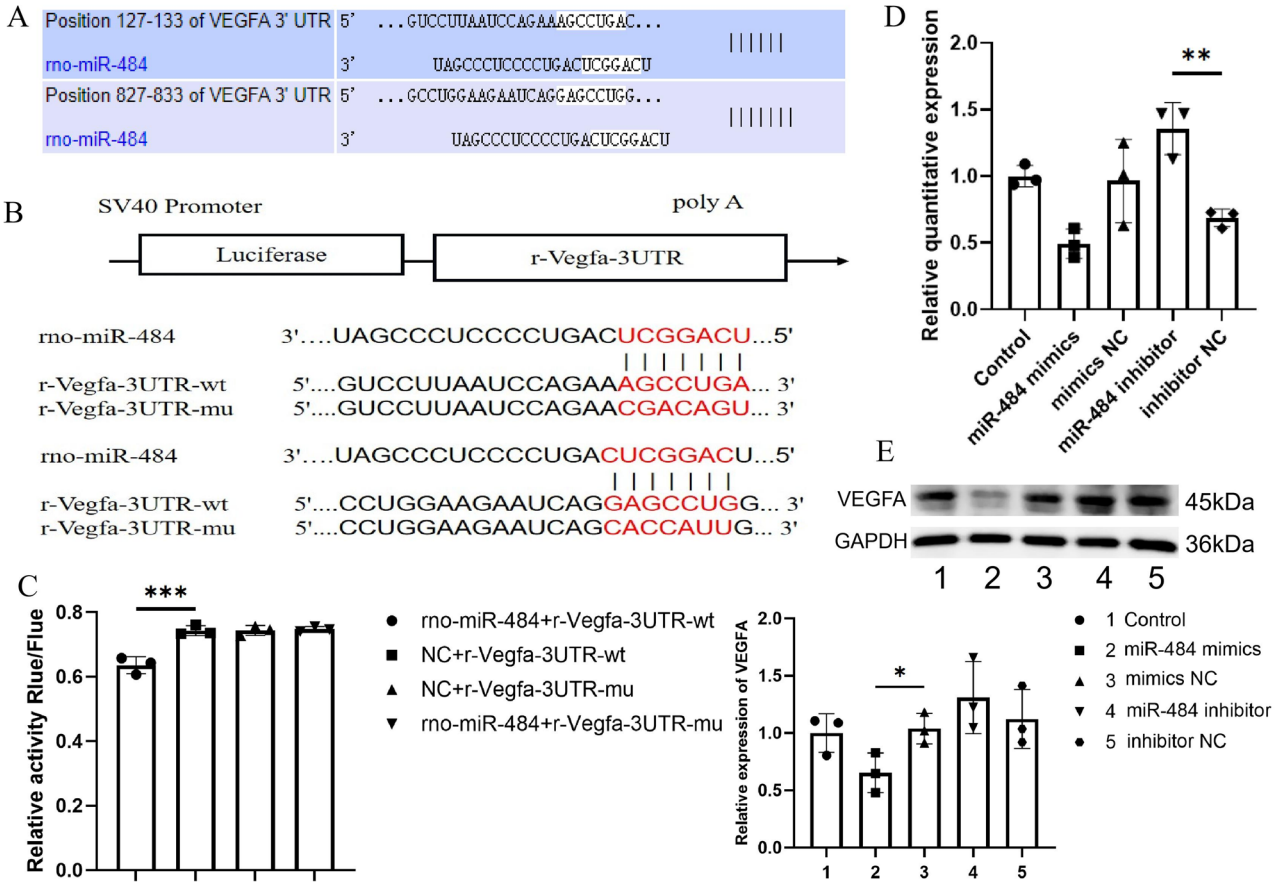

Fig. 7 miR-484 directly targets VEGFA. **A** rno-miR-484 binding sites within the r-vegfa-3'UTR. **B** Diagram of the binding of rno-miR-484 to target sites of the r-vegfa-3'UTR. **C** Dual luciferase reporter assay for the interaction between rno-miR-484 and the r-vegfa-3'UTR. $n=3$, 0.636 ± 0.026 vs. 0.743 ± 0.015, ***$P<0.001$ compared with the NC + r-Vegfa-3UTR-wt group. **D** Effect of miR-484 on VEGF mRNA expression. $n=3$, 1.358 ± 0.203 vs. 0.687 ± 0.072, **$P=0.008$, compared with inhibitor NC. **E** Effect of miR-484 on VEGF protein expression. $n=3$, 0.652 ± 0.173 vs. 1.039 ± 0.134, *$P=0.038$, compared with mimics NC. Values are the means ± SDs

systemic regulation, which aligns with enhanced angiogenesis post-MI. Conversely, in vitro models, by isolating the hypoxic stimulus and excluding confounding factors, demonstrate a hypoxia-induced upregulation of miR-484 that directly inhibits endothelial cell angiogenesis through the VEGFA signaling pathway. In vivo, the downregulation of miR-484 may mediate the enhancement of VEGFA-dependent pro-angiogenic effects after MI, thereby promoting cardiac repair.

According to the results of the target gene prediction and pathway analysis for miR-484, calcium ion channels have garnered attention due to their close association with angiogenesis [29]. Through protein interaction analysis, we identified that the two molecules, RYR2 and CACNA1D, are crucial. Both of these molecules are calcium ion release channels. Literature review showed that RyR participates in the calcium signaling of human aortic endothelial cells induced by VEGF, and that inhibiting RyR with ryanodine can prevent the VEGF-stimulated Ca^{2+} influx [30]. Therefore, we conjecture that miR-484 may target RYR2, contributing to the calcium signaling in human endothelial cells induced by VEGF.

In various diseases, the dysregulation of miRNAs reflects the disorders affecting the cellular processes. MiRNAs have been shown to bind to the 3' untranslated regions (UTRs) of messenger RNAs (mRNAs), leading to mRNA degradation and translation repression [31]. Our findings, in combination with the results of bioinformatics analyses and previous studies, indicate that VEGFA is a promising candidate target for miR-484. The luciferase reporter assay results confirmed that miR-484 could directly target VEGFA. Furthermore, the expression of VEGFA mRNA was inhibited by the overexpression of miR-484 in HUVECs, suggesting that exosomal miR-484 potentially inhibits angiogenesis by targeting VEGFA, which deserves further investigation.

The VEGF–VEGF receptor (R) system is essential for diverse physiological processes [32]. Phosphatidylinositol 3-kinase (PI3K) and mitogen-activated protein kinase (MAPK) signaling are activated after the

autophosphorylation of VEGFR [33]. Functionally, VEGFA has been documented to have crucial function in angiogenesis [34] by controlling the maturation of endothelial progenitor cells, enhancing the growth and movement of endothelial cells, and augmenting vascular permeability. Aligning with the results of other studies, miR-484 can impede tumor progression and angiogenesis by directly interacting with VEGFA in ovarian cancer. Furthermore, small molecule inhibitors selectively targeting VEGFR can inhibit tumor growth and angiogenesis in epithelial cancer [35–37].

This study has some limitations. The sample size used in this study is relatively small, which may affect the statistical power and reliability of some of the results. Nevertheless, we have employed strict randomization and blinding procedures in the experimental design and used appropriate statistical methods to minimize bias and ensure the reliability of the data. However, the limitation of sample size may affect the generalizability and applicability of the results. Future studies can validate the robustness and reliability of the findings by increasing the sample size. Beisides, Although this study only used the H9C2 cell line for exosome isolation and analysis, previous research [38] has shown that the exosomes secreted by H9C2 cells and primary cardiomyocytes are highly similar in size, morphology, and function, including the ability to induce endothelial cell proliferation and angiogenesis. Based on this evidence, we believe that the results of H9C2 exosomes obtained in this study are of some reference value. However, we also acknowledge that further validation using primary cardiomyocytes is needed in future studies and investigate the effects of exosomes derived from miR-484 -knockdown H9C2 cells on HUVECs. Although this study indicates that miRNAs in serum exosomes after MI may play a role in angiogenesis, the specific source of exosomes remains unclear. The miRNAs contained in the serum exosomes we isolated may originate from various cell types, including cardiomyocytes, immune cells, and other cells involved in the repair process after MI. Future studies can verify the specific source of serum exosomes and explore the different regulatory effects of exosomal miRNAs from different cell types on angiogenesis and other biological processes using cell labeling techniques or more precise source tracking methods. The exosome characterization in this study mainly relies on the analysis of transmembrane protein markers (CD63, CD81) and physical properties. Future studies will incorporate a more comprehensive panel of markers, such as TSG101, Alix, and other cytosolic proteins, as well as negative controls like Calnexin, in accordance with the ISEV2018 guidelines for stricter identification.

In conclusion, this study identified differentially expressed exosomal miRNAs between MI model and control rats, providing new data for exploring the regulatory role and therapeutic potential of exosomal miRNAs in MI. This study lays the foundation for subsequent cell experiments. The specific role and mechanism of these miRNA molecules in exosomes in the occurrence, development, prevention, and treatment of angiogenesis after MI could be further explored.

Supplementary Information

The online version contains supplementary material available at https://doi.org/10.1186/s12872-026-05750-8.

Supplementary Material 1.

Supplementary Material 2.

Supplementary Material 3.

Supplementary Material 4.

Supplementary Material 5.

Supplementary Material 6.

Acknowledgements
Not application.

Authors' contributions
DD.W., R.Y. and X.C. made substantial contributions to conception and design, acquisition of data, or analysis and interpretation of data. QQ.G. and YJ.G. took part in drafting the article or revising it critically for important intellectual content. M.C. and DM.Z. provided financial support, experimental design, and manuscript revision. All authors gave final approval of the version to be published, and agreed to be accountable for all aspects of the work.

Funding
The authors gratefully acknowledge the financial support from the National Natural Science Foundation of China (No. 81973780) and Fundamental Research Funds for the Central Universities (2019-BUCMXJKT017).

Data availability
The datasets generated and/or analyzed during the current study are not publicly available due to confidentiality, but are available from the corresponding author on reasonable request.

Declarations

Ethics approval and consent to participate
This study was supported by the Animal Ethics Committee of Dongzhimen Hospital, Beijing University of Chinese Medicine (No. 19 – 02).

Consent for publication
Not application.

Competing interests
The authors declare no competing interests.

Author details
[1]Key Laboratory of Chinese Internal Medicine of Ministry of Education and Beijing, Dongzhimen Hospital, Beijing University of Chinese Medicine, Beijing 100700, China
[2]College of Traditional Chinese Medicine, Xinjiang Medical University, Xinjiang 830011, China
[3]School of Traditional Chinese Medicine, Beijing University of Chinese Medicine, Beijing 100029, China

Received: 10 December 2024 / Accepted: 13 March 2026
Published online: 23 March 2026

References

1. Tsao CW, Aday AW, Almarzooq ZI, et al. Heart Disease and Stroke Statistics-2023 Update: A Report From the American Heart Association. Circulation. 2023;147(8):e93–621. https://doi.org/10.1161/cir.0000000000001123.
2. Santos-Zas I, Lemarié J, Zlatanova I, et al. Cytotoxic CD8(+) T cells promote granzyme B-dependent adverse post-ischemic cardiac remodeling. Nat Commun. 2021;12(1):1483. https://doi.org/10.1038/s41467-021-21737-9.
3. Lee MS, Park HS, Lee BC, Jung JH, Yoo JS, Kim SE. Identification of Angiogenesis Rich-Viable Myocardium using RGD Dimer based SPECT after Myocardial Infarction. Sci Rep. 2016;6:27520. https://doi.org/10.1038/srep27520.
4. Bentsen S, Jensen JK, Christensen E, et al. [(68)Ga]Ga-NODAGA-E[(cRGDyK)](2) angiogenesis PET following myocardial infarction in an experimental rat model predicts cardiac functional parameters and development of heart failure. J Nucl Cardiol. 2023;30(5):2073–84. https://doi.org/10.1007/s12350-023-03265-9.
5. Cazzanelli P, Wuertz-Kozak K. MicroRNAs in Intervertebral Disc Degeneration, Apoptosis, Inflammation, and Mechanobiology. Int J Mol Sci. 2020;21(10). https://doi.org/10.3390/ijms21103601.
6. Tiwari A, Mukherjee B, Dixit M. MicroRNA Key to Angiogenesis Regulation: MiRNA Biology and Therapy. Curr Cancer Drug Targets. 2018;18(3):266–77. https://doi.org/10.2174/1568009617666170630142725.
7. Chi F, Feng L, Li Y, et al. MiR-30b-5p promotes myocardial cell apoptosis in rats with myocardial infarction through regulating Wnt/β-catenin signaling pathway. Minerva Med. 2023;114(4):476–84. https://doi.org/10.23736/s0026-4806.20.06565-9.
8. Jang J, Song G, Pettit SM, et al. Epicardial HDAC3 Promotes Myocardial Growth Through a Novel MicroRNA Pathway. Circ Res. 2022;131(2):151–64. https://doi.org/10.1161/circresaha.122.320785.
9. Davidson SM, Boulanger CM, Aikawa E, et al. Methods for the identification and characterization of extracellular vesicles in cardiovascular studies: from exosomes to microvesicles. Cardiovasc Res. 2023;119(1):45–63. https://doi.org/10.1093/cvr/cvac031.
10. Wen H, Peng L, Chen Y. The effect of immune cell-derived exosomes in the cardiac tissue repair after myocardial infarction: Molecular mechanisms and pre-clinical evidence. J Cell Mol Med. 2021;25(14):6500–10. https://doi.org/10.1111/jcmm.16686.
11. Guo D, Yan J, Yang Z, et al. The immune regulatory role of exosomal miRNAs and their clinical application potential in heart failure. Front Immunol. 2024;15:1476865. https://doi.org/10.3389/fimmu.2024.1476865.
12. Liu W, Li L, Rong Y, et al. Hypoxic mesenchymal stem cell-derived exosomes promote bone fracture healing by the transfer of miR-126. Acta Biomater. 2020;103:196–212. https://doi.org/10.1016/j.actbio.2019.12.020.
13. Fang Y, Ni J, Wang YS, et al. Exosomes as biomarkers and therapeutic delivery for autoimmune diseases: Opportunities and challenges. Autoimmun Rev. 2023;22(3):103260. https://doi.org/10.1016/j.autrev.2022.103260.
14. Kainuma S, Miyagawa S, Fukushima S, et al. Influence of coronary architecture on the variability in myocardial infarction induced by coronary ligation in rats. PLoS ONE. 2017;12(8):e0183323. https://doi.org/10.1371/journal.pone.0183323.
15. Guo Q, Wu D, Jia D, et al. Bioinformatics prediction and experimental verification of a novel microRNA for myocardial fibrosis after myocardial infarction in rats. PeerJ. 2023;11:e14851. https://doi.org/10.7717/peerj.14851.
16. Osuru HP, Lavallee M, Thiele RH. Molecular and Cellular Response of the Myocardium (H9C2 Cells) Towards Hypoxia and HIF-1α Inhibition. Front Cardiovasc Med. 2022;9:711421. https://doi.org/10.3389/fcvm.2022.711421.
17. Sabui S, Ramamoorthy K, Romero JM, Simoes RD, Fleckenstein JM, Said HM. Hypoxia inhibits colonic uptake of the microbiota-generated forms of vitamin B1 via HIF-1α-mediated transcriptional regulation of their transporters. J Biol Chem. 2022;298(2):101562. https://doi.org/10.1016/j.jbc.2022.101562.
18. Zhao Z, Shuang T, Gao Y, et al. Targeted delivery of exosomal miR-484 reprograms tumor vasculature for chemotherapy sensitization. Cancer Lett. 2022;530:45–58. https://doi.org/10.1016/j.canlet.2022.01.011.
19. Califano D, Gallo D, Rampioni Vinciguerra GL, et al. Evaluation of Angiogenesis-Related Genes as Prognostic Biomarkers of Bevacizumab Treated Ovarian Cancer Patients: Results from the Phase IV MITO16A/ManGO OV-2 Translational Study. Cancers (Basel). 2021;13(20). https://doi.org/10.3390/cancers13205152.
20. Das CK, Jena BC, Banerjee I, et al. Exosome as a Novel Shuttle for Delivery of Therapeutics across Biological Barriers. Mol Pharm. 2019;16(1):24–40. https://doi.org/10.1021/acs.molpharmaceut.8b00901.
21. Yu X, Odenthal M, Fries JW. Exosomes as miRNA Carriers: Formation-Function-Future. Int J Mol Sci. 2016;17(12). https://doi.org/10.3390/ijms17122028.
22. Hu Y, Rao SS, Wang ZX, et al. Exosomes from human umbilical cord blood accelerate cutaneous wound healing through miR-21-3p-mediated promotion of angiogenesis and fibroblast function. Theranostics. 2018;8(1):169–84. https://doi.org/10.7150/thno.21234.
23. Lu W, Liu X, Zhao L, et al. MiR-22-3p in exosomes increases the risk of heart failure after down-regulation of FURIN. Chem Biol Drug Des. 2023;101(3):550–67. https://doi.org/10.1111/cbdd.14142.
24. Li Y, Liu Y, Yao J, Li R, Fan X. Downregulation of miR-484 is associated with poor prognosis and tumor progression of gastric cancer. Diagn Pathol. 2020;15(1):25. https://doi.org/10.1186/s13000-020-00946-8.
25. Miyazawa R, Iso Y, Tsujiuchi M, et al. Potential Association of Circulating MicroRNA-181c and MicroRNA-484 Levels with Cardiorespiratory Fitness after Myocardial Infarction: A Pilot Study. Prog Rehabil Med. 2021;6:20210017. https://doi.org/10.2490/prm.20210017.
26. Liu H, Li S, Jiang W, Li Y. MiR-484 Protects Rat Myocardial Cells from Ischemia-Reperfusion Injury by Inhibiting Caspase-3 and Caspase-9 during Apoptosis. Korean Circ J. 2020;50(3):250–63. https://doi.org/10.4070/kcj.2019.0107.
27. Zielińska W, Zabrzyński J, Gagat M, Grzanka A. The Role of TRPM2 in Endothelial Function and Dysfunction. Int J Mol Sci. 2021;22(14):7635. https://doi.org/10.3390/ijms22147635.
28. Jiang M, Lin L, Yue S, et al. Mitochondrial Calcium Uniporter-Mediated Regulation of the SIRT3/GSK3β/β-Catenin Signaling Pathway in Vascular Remodeling. FASEB J. 2025;39(13):e70761. https://doi.org/10.1096/fj.202500369RR.
29. Pham DL, Niemi A, Ko ML, Ko GYP. Peptide Lv augments intermediate-conductance calcium-dependent potassium channels (KCa3.1) in endothelial cells to promote angiogenesis. PLoS ONE. 2022;17(10):e0276744. https://doi.org/10.1371/journal.pone.0276744.
30. Evangelista AM, Thompson MD, Weisbrod RM, et al. Redox regulation of SERCA2 is required for vascular endothelial growth factor-induced signaling and endothelial cell migration. Antioxid Redox Signal. 2012;17(8):1099–108. https://doi.org/10.1089/ars.2011.4022.
31. Kiltschewskij DJ, Harrison PF, Fitzsimmons C, Beilharz TH, Cairns MJ. Extension of mRNA poly(A) tails and 3'UTRs during neuronal differentiation exhibits variable association with post-transcriptional dynamics. Nucleic Acids Res. 2023;51(15):8181–98. https://doi.org/10.1093/nar/gkad499.
32. Apte RS, Chen DS, Ferrara N. VEGF in Signaling and Disease: Beyond Discovery and Development. Cell. 2019;176(6):1248–64. https://doi.org/10.1016/j.cell.2019.01.021.
33. Wiszniak S, Schwarz Q. Exploring the Intracrine Functions of VEGF-A. Biomolecules. 2021;11(1). https://doi.org/10.3390/biom11010128.
34. Zhou Y, Zhu X, Cui H, et al. The Role of the VEGF Family in Coronary Heart Disease. Front Cardiovasc Med. 2021;8:738325. https://doi.org/10.3389/fcvm.2021.738325.
35. Cai D, Chen C, Su Y, Tan Y, Lin X, Xing R. LRG1 in pancreatic cancer cells promotes inflammatory factor synthesis and the angiogenesis of HUVECs by activating VEGFR signaling. J Gastrointest Oncol. 2022;13(1):400–12. https://doi.org/10.21037/jgo-21-910.
36. El-Fakharany ZS, Nissan YM, Sedky NK, Arafa RK, Abou-Seri SM. New proapoptotic chemotherapeutic agents based on the quinolone-3-carboxamide scaffold acting by VEGFR-2 inhibition. Sci Rep. 2023;13(1):11346. https://doi.org/10.1038/s41598-023-38264-w.
37. Modi SJ, Kulkarni VM. Discovery of VEGFR-2 inhibitors exerting significant anticancer activity against CD44 + and CD133 + cancer stem cells (CSCs): Reversal of TGF-β induced epithelial-mesenchymal transition (EMT) in hepatocellular carcinoma. Eur J Med Chem. 2020;207:112851. https://doi.org/10.1016/j.ejmech.2020.112851.
38. Ribeiro-Rodrigues TM, Laundos TL, Pereira-Carvalho R, et al. Exosomes secreted by cardiomyocytes subjected to ischaemia promote cardiac angiogenesis. Cardiovasc Res. 2017;113(11):1338–50. https://doi.org/10.1093/cvr/cvx118.

Publisher's Note